PCCP

PAPER

View Article Online
View Journal | View Issue

Cite this: *Phys. Chem. Chem. Phys.*, 2024, **26**, 28161

Substitutional control of non-statistical dynamics in the thermal deazetization of tetracyclic azo compounds†

Chandralekha Hajra and Ayan Datta *

Dynamical control of reactivity for the deazetization of *endo*,*endo*-9,10-diazatetracyclo[3.3.2.0^{2,4}.0^{6,8}]dec-9-ene (**3**) is studied using on-the-fly quasi-classical trajectory (QCT) calculations at the density functional theory (DFT) level. Two degenerate homotropilidenes, **4** and **5**, are formed simultaneously from a single transition state (TS). The ratio of the cyclohexadienyl substituted product, **4**, and the dynamical product, *i.e.* bridgehead substituted product, **5**, can be neatly controlled by tuning the topology of the potential energy surface (PES). A steep descent post-TS favors the cyclohexadienyl substituted product while a shallow descent increases the dynamical outcome. Chemical demonstration of the same is achieved by symmetrical and asymmetrical substitution of functional groups along the cleaving (C3–C4) bond. Asymmetric mono-functionalization makes the PES broader, thereby reducing the slope post-TS. This creates a favourable situation for the dynamical products, **5b–5d**, to become the major ones. On the contrary, symmetric bi-functionalization makes the cyclohexadienyl substituted product, **4m–4o**, overwhelmingly (>85%) predominating. As a corollary to this phenomenon, substitution of the C3–C4 bond by the heavier isotopologues of H/C restricts its motion along the IRC path by the Newtonian kinetic isotope effect. This facilitates bond-opening along the C10–C11 dynamical pathway. Hence, for isotopic substitution, the situation is reversed and the bifunctionalized **3** is more dynamically activated. Simultaneous substitution by the heavier isotopologue of C and H causes deviation from the geometric mean of individual isotopic substitution towards the dynamical product, **5**. Therefore, the dynamic control in **3** becomes prominent either *via* functional group asymmetry or through a Newtonian kinetic isotope effect for symmetric bifunctionalization.

Received 3rd September 2024,
Accepted 22nd October 2024

DOI: 10.1039/d4cp03447c

rsc.li/pccp

Introduction

Cyclic azo alkanes constitute a versatile class of organic compounds characterized by the presence of one or more azo functional groups. The diverse applications of these compounds arise from both the number of rings and their respective sizes. Their utility spans dyeing, pigment production, and the development of photochromic materials, among others.[1–3] They have the ability to exist in different isomeric forms, dictated by the orientation of the rings relative to the azo group and other functional groups attached to the ring. This imparts significant diversity in their reactivity.[4] The inherent reactivity of cyclic azo compounds depends critically on the strain within the rings. This enables them to undergo deazetization reactions wherein cleavage of the azo group occurs, further expanding their synthetic possibilities.[5]

The smallest amongst the cyclic rings, cyclopropenes, show high reactivity in bioorthogonal reactions due to their highly strained structure. Recently, cyclopropene derivatives have gained huge attention as they have small sizes and hydrophobic properties. The rapid and selective reaction kinetics of tetrazine derivatives with cyclopropenes have been utilized for imaging purposes owing to the high contrast and minimal background signal.[6,7] Inverse-electron demand Diels–Alder reactions between tetrazines and strained alkenes or alkynes have been reviewed by Boger.[8] This results in the formation of dihydropyridazines or pyridazines with nitrogen gas being the sole byproduct. Prescher and co-workers have observed isomeric cyclopropenes displaying a variety of reactivities with tetrazines.[9] Even though in general cyclopropenes do not react with tetrazine, Sauer and co-workers could form highly strained 3,4-diazanorcaradienes and 9,10-diazatetracyclo[3.3.2.0^{2,4}.0^{6,8}]dec-9-ene from the reaction of cyclopropene with tetrazines.[10,11]

Elimination of the azo-group from 9,10-diazatetracyclo[3.3.2.0^{2,4}.0^{6,8}]dec-9-ene (3) produces homotropilidenes. They show unique chemical reactivity because of their strained

---

School of Chemical Sciences, Indian Association for the Cultivation of Science, 2A and 2B Raja S. C. Mullick Road, Jadavpur – 700032, Kolkata, West Bengal, India. E-mail: spad@iacs.res.in; Tel: +91-33-24734971

† Electronic supplementary information (ESI) available: Cartesian coordinates, energies, and harmonic frequencies, free-energy barriers, calculations for NBO analyses and QCT input. See DOI: **https://doi.org/10.1039/d4cp03447c**

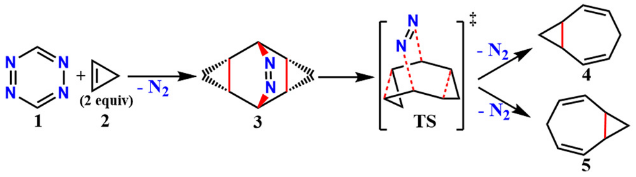

Scheme 1 Formation of homotropilidenes through deazetization reaction from **3**.

structure.[12,13] Scheme 1 shows the formation of **3** by the [4+2] cycloaddition of symmetric electron-deficient tetrazines (**1**) with two equivalents of cyclopropenes (**2**).[14] Thermolysis of **3** produces homotropilidenes (**4** and **5**) through the elimination of a N_2 molecule. The degeneracy between **4** and **5** can be broken to selectively prefer either of them based on the substituents on **3**. The overall pathway along **1** → **4,5** is significantly thermodynamically downhill, which drives spontaneous product formation (see ESI,† Fig. S1).

One of the more popular frameworks to understand the selectivity of products is the transition state theory (TST) or variational transition state theory (VTST). Within this model, products are formed through competing independent transition-states and the free-energy difference amongst them can be utilized for a quantitative comprehension of the origin of product selectivity.[15,16] However, an alternative product selectivity might arise when two products originate from a single transition state. In this scenario, the pathway of products shares a transition state, diverging after the valley-ridge inflection point when the potential energy surface bifurcates. Therefore, in such cases, post-TS effects like the vibrational motion and momenta of atoms along the non-intrinsic reaction coordinate (non-IRC) pathways become predominant.[17–20] Tantillo *et al.* have studied post-TS bifurcations on several organic reactions.[19–23] Houk and co-workers have studied non-statistical molecular dynamical effects in deazetization reaction of azoalkanes.[24,25] Dynamical effects have been shown to be essential to describe the high selectivity in the [3,3] sigmatropic rearrangement for bispercyclic transition-state.[26] Post-transition-state dynamics have been shown to be important for reactions in which the number of concerted processes is more than 3.[27] Ess and co-workers have studied the nonstatistical intermediates and dynamically regulated routes for benzene reductive elimination from Mo/W-based organometallic complexes using direct-dynamics simulations.[28] Mandal *et al.* have shown that deazetization reactions for semibullvalene formation, Au(I)-catalysed intramolecular Diels–Alder processes and the valence isomerism in benzene imine are richly controlled dynamical effects.[29–31]

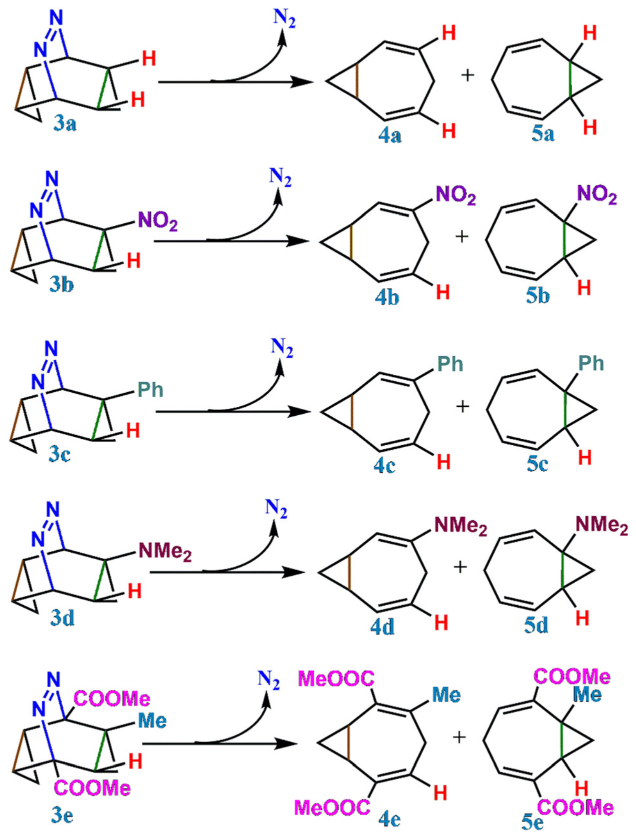

Fig. 1 Formation of homotropilidenes (**4** and **5**) from *endo,endo*-9,10-diazatetracyclo[3.3.2.0^{2,4}.0^{6,8}]dec-9-ene (**3**) through deazetization reaction.

The mechanism for the thermolysis of azo compounds is of importance[32,33] and therefore, the thermolysis of **3** to form **4** and **5** is studied in the present article. The IRC and non-IRC preferences for **4** or **5** are investigated computationally by substituting functional groups (Fig. 1) on **3**. Additionally, we carried out detailed quasiclassical trajectory simulations from the ambimodal transition state structure to examine dynamical behaviour. Newtonian kinetic isotope effects (KIEs)[34] were computed to assess the kinetic selectivity *via* isotope labelling.

Computational details

The structures for each molecule, along with the harmonic frequencies were computed using the Gaussian 16 program[35] at the M06-2X/6-31G(d) level of theory.[36,37] To ensure that transition states connect to the desirable stationary-points, intrinsic reaction coordinate (IRC) calculations were performed.[38] Benchmarking of these calculations was performed at various levels of theory, including the B3LYP/6-31G(d), B3LYP/6-31+G(d,p) with dispersion corrections using Grimme's D3, and M06-2X/6-31+G(d,p) for a comparison of different theoretical methods.[39–41] Additionally, single-point calculations were also performed at the DLPNO-CCSD(T)[42,43]/def2-TZVP level to further validate the DFT results (see ESI,† Table S1).[44] Calculations at the DLPNO-CCSD(T)/def2-TZVP level are also in agreement with the DFT calculations. DLPNO-CCSD(T) calculations are done in ORCA 5.0.[45] The 3D-view of the molecular structures was retrieved using Gauss View 6.1.1, a popular visualization tool that aids in the accurate depiction and analysis of complex molecular geometries.

The quasiclassical trajectories (QCTs) were simulated *via* on-the-fly molecular dynamics (MD) using Singleton's ProgDyn code interfaced with Gaussian16, which calculates the force

Table 1 Relative reaction enthalpy, free energy, activation enthalpy and free energy activations at 298.15 K (in kcal mol^{-1}) for **3(a–d)** → **4(a–d)** and **3(a–d)** → **5(a–d)** at the M06-2X/6-31G(d) level of theory

	ΔH	ΔG	$\Delta H^{\ddagger}_{3\to4}$	$\Delta G^{\ddagger}_{3\to4}$	$\Delta H^{\ddagger}_{4\to5}$	$\Delta G^{\ddagger}_{4\to5}$
3a → **4a**	−51.0	−64.2	8.2	8.3	15.5	16.2
3a → **5a**	−51.0	−64.2				
3b → **4b**	−52.7	−66.4	8.0	7.7	14.8	16.1
3b → **5b**	−52.5	−65.6				
3c → **4c**	−52.2	−65.0	8.7	8.4	15.5	16.2
3c → **5c**	−50.2	−63.5				
3d → **4d**	−50.9	−64.0	9.2	9.1	16.6	19.1
3d → **5d**	−50.3	−63.3				

constant at each time-step along with trajectory formation at the M06-2X/6-31G(d) level of theory.[46] ProgDyn generates the initial geometries from the precise frequency calculations based on the optimized transition state structures. All direct MD simulations were conducted at 298.15 K to mimic realistic reaction conditions. Normal mode sampling involved adding the zero-point energies for each real normal mode of the transition state, followed by Boltzmann sampling to generate a comprehensive set of coordinates for trajectory propagation. In these simulations, molecular configurations and velocities were propagated in both the forward and backward directions using the velocity Verlet algorithm with a timestep of 1 fs. This method ensured accurate propagation until either the starting material or the product was obtained. At each time step, the nuclei were propagated classically, while the electronic structures were calculated quantum mechanically using DFT (M06-2X/6-31G(d) level). Detailed thresholds for bond formations and trajectory terminations are provided in the ESI† for a reproducible workflow for these simulations.

Results and discussion

As shown in Table 1, the formation of both the homotropilidenes, **4** and **5**, is thermodynamically favourable. For **3a**, both **4a** and **5a** are degenerate but when a functional group is substituted on **3**, the degeneracy of **4** and **5** is lifted making **4** relatively more stable than **5**. The preferential stability of **4** can be understood by the electron-withdrawing/electron-donating properties of the substituents as well as steric effects. In the case of **4b** and **5b**, a H atom is substituted by the electron withdrawing $-NO_2$ group which increases the s-character of the adjacent bond resulting in an enhanced bond-angle within the cyclopropane ring. This makes **5b** relatively unstable (see, ESI,† Tables S2 and S3 for the % s-character from NBO analysis). For **4c**, **5c** and **4d**, **5d**, the $-NMe_2$ and phenyl groups have +R effect. Both the groups are able to delocalize the electron-density on adjacent double-bonds. Therefore, **4c** and **4d** get stabilized.

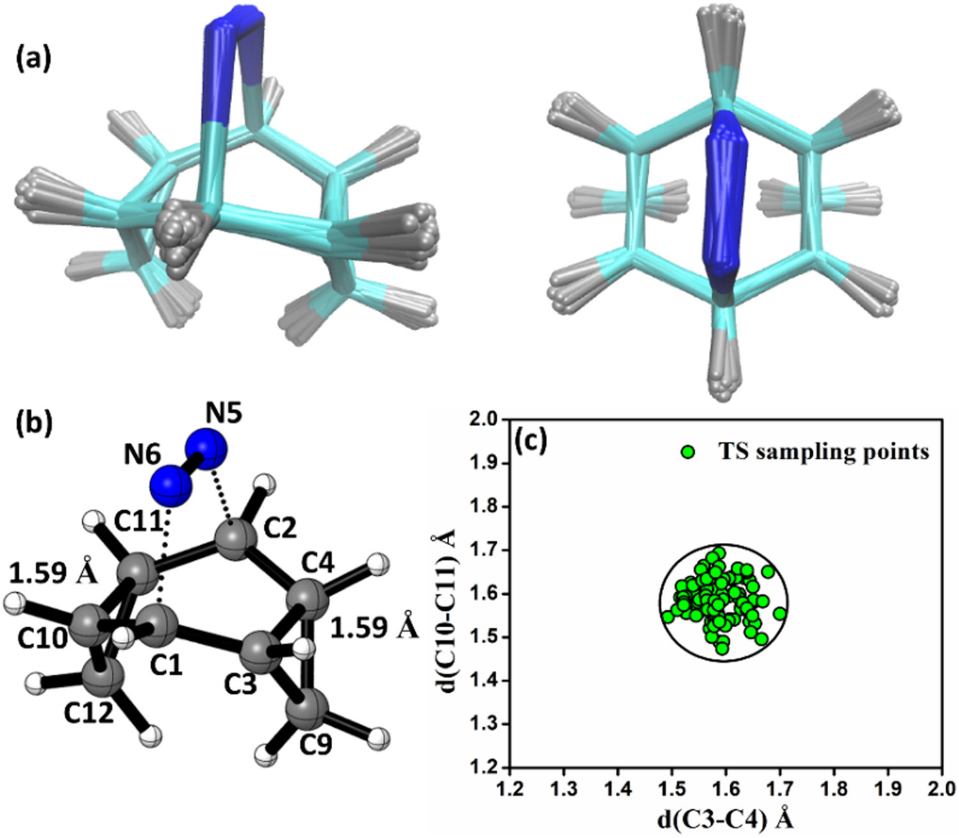

Fig. 2 (a) Side and top views of the overlay of 30 sampled TS structures, **TS-a**. (b) Transition-state (**TS-a**) obtained along the IRC path between **3a** and **4a** at the M062X/6-31G(D) level of theory. (c) Scatter plot in C3–C4 and C10–C11 bond lengths across 100 sampled TS (**TS-a**) structures.

TS (**3** → **4**,**5**) involves the N_2 elimination reaction. The free-energy barrier, $\Delta G^{\ddagger}_{\mathbf{3}\rightarrow\mathbf{4,5}}$ for **3b** is the lowest in the series which again is correlated with the smaller % s – character of C–N making it weaker for easy dissociation. The barrier for the **4** → **5** interconversion is significantly higher than the initial product formation barrier. It is worthwhile to mention here that the *endo* conformers of **3(a–d)** are considered here for the thermal deazetization reactions as the barriers are significantly higher for the same in the cases of the *exo*-conformers, $\mathbf{3}^{\#}$ (see ESI,† Table S10). Houk and co-workers have found that the high thermal barrier in the case of the *exo*-conformers is due to the di-radical nature of the transition-states.[24] In fact, deazetization reactions for the *exo*-conformers occur exclusively under photochemical conditions.[10–13]

The steepest decent path from **3** *via* **TS** in mass-weighted coordinates with infinitesimal atomic velocity as represented by intrinsic reaction coordinate (IRC) calculations connects to **4**. For reactant **3a**, products **4a** and **5a** are the same. However for transition states **TS(b–d)**, IRC connects **3(b–d)** to the more stable **4(b–d)**. For **3(a–d)**, the valley-ridge inflection (VRI) point is found on the right-hand side of the transition-state that is towards the product. In all cases, only product **4** is obtained from IRC calculations except for degenerate **3a** which connects **TS** with $\mathbf{TS_{4\rightarrow5}}$. Nevertheless, previous experiments on similar reactions have shown that both the products, namely **4** and **5**, are found. Additionally from Table 1, it is clear that the reaction barrier from **4** to **5** $\left(\Delta G^{\ddagger}_{\mathbf{4}\rightarrow\mathbf{5}}\right)$ is much higher ($\sim$15–19 kcal mol^{-1}) than $\Delta G^{\ddagger}_{\mathbf{3}\rightarrow\mathbf{4,5}}$. Therefore, the thermal interconversion from the cyclohexadienyl substituted product (**4**) to the bridgehead substituted product (**5**) is unlikely at room temperature. This implies that there must be a post transition-state bifurcation on PES. As shown in Scheme 1, the **TS** bifurcates into **4** or **5**. The bifurcation of PES is caused at the VRI point beyond which trajectories have an option to reach alternative products.

In this regard, we have conducted quasi-classical trajectory (QCT) analyses in the gas-phase. Since the species involved in the reaction are not overtly polar, consideration of implicit polar solvent models should not affect the path significantly. The results of the implicit solvation model of the barriers are reported in Tables S7–S9 (ESI†). The M06-2X/6-31G(d) level of theory is employed for all the trajectory propagations. Trajectories were initiated from transition-state ensembles of **TS** created using ProgDyn and propagated *via* classical equations of motion, with forces calculated quantum-mechanically in real-time. Transition-state ensembles were generated by performing Boltzmann sampling of geometries using normal-mode sampling, adding zero-point energy for each real normal mode, and incorporating thermal energy at 298 K to the structures. To verify the robustness of the sampling method, we have plotted an overlay of 30 sampled transition-state structures of **TS** and plotted the C3–C4 *vs.* C10–C11 bonds of 100 sampled transition state structures of **TS** in Fig. 2. We can see that the transition-state structure lies in a zone for which bond lengths are 1.59 ± 0.004 Å. 98% of transition-state bond lengths are in this region.

To determine selectivity between products **4** and **5**, MD reaction trajectory calculations have been performed. Amongst a total of 363 trajectories that were propagated, 336 (92%) were productive for **3a**. Within the productive trajectories, 163 (44.9%) form product **4a** while 173 (47.7%) reached product **5a** and only 5 (1.5%) trajectories went through $\mathbf{TS_{4a\rightarrow5a}}$ to reach either **4a** or **5a**. This is in agreement with the intuitive expectation for degenerate product formation producing a numerical **4a** : **5a** (1 : 1.06) ratio $\sim$1. From Table 2, we can see that for the reactant **3b** where the substitutional degeneracy is broken, the product ratio between **4b** and **5b** gets altered from unity. In fact, the bridgehead substituted product, **5b**, becomes the major product. Even larger population of the bridgehead substituted product is observed in **3c**. **3d** also shows that the bridgehead substituted product is major (Fig. 3).

In the case of **3a**, the average time to reach TS (**TS-a**) from reactant (**3a**) is 58.38 ± 2.87 fs and the times taken to form product **4a** from **TS-a** and **5a** from **TS-a** are almost equal. For **4a**, it is 90 ± 3.36 fs and for **5a** it is 95.29 ± 4.19 fs. Therefore, for the degenerate products **4a** and **5a** the potential energy surfaces after bifurcation are identical making the product-ratio $\sim$1. For **3b**, the time to reach **TS-b** from **3b** is 59.19 ± 2.77 fs and the times to form product **4b** and **5b** are 102.23 ± 3.38 fs and 91.29 ± 2.41 fs, respectively. The faster formation of the bridgehead substituted product explains its higher population. **3c** forms **5c** (t = 79.77 ± 1.45 fs) faster than **4c** (t = 90.96 ± 2.23 fs). **3d** requires 94.03 ± 3.16 fs and 85.26 ± 1.96 fs to form the cyclohexadienyl substituted and bridgehead substituted products, respectively. For all the cases (**3a–3d**), one observes at-least 50% bridgehead substituted products. What accounts for such pronounced non-IRC behaviour in these reactions?

To address this, we have further studied the dynamical (bridgehead substituted product) and cyclohexadienyl substituted product distributions in a series of mono and bi-substitutionally modified *endo*,*endo*-9,10-diazatetracyclo[$3.3.2.0^{2,4}.0^{6,8}$]dec-9-ene (**3e–3o**) in Table 3. The presence of two functional groups on the same side makes the reactions

Table 2 Trajectory analyses at 298.15 K for **3(a–d)** → **4(a–d)** and **3(a–d)** → **5(a–d)** at the M06-2X/6-31G(d) level of theory

Reactant	Total trajectories	Productive trajectories	Trajectories reaching **4** (IRC) (cyclohexadienyl substituted product)	Trajectories reaching **5** (dynamical) (bridgehead substituted product)	**4** : **5**
3a	363	336	163	173	1 : 1.06
3b	431	394	186	208	1 : 1.12
3c	786	720	320	400	1 : 1.25
3d	506	476	224	252	1 : 1.12

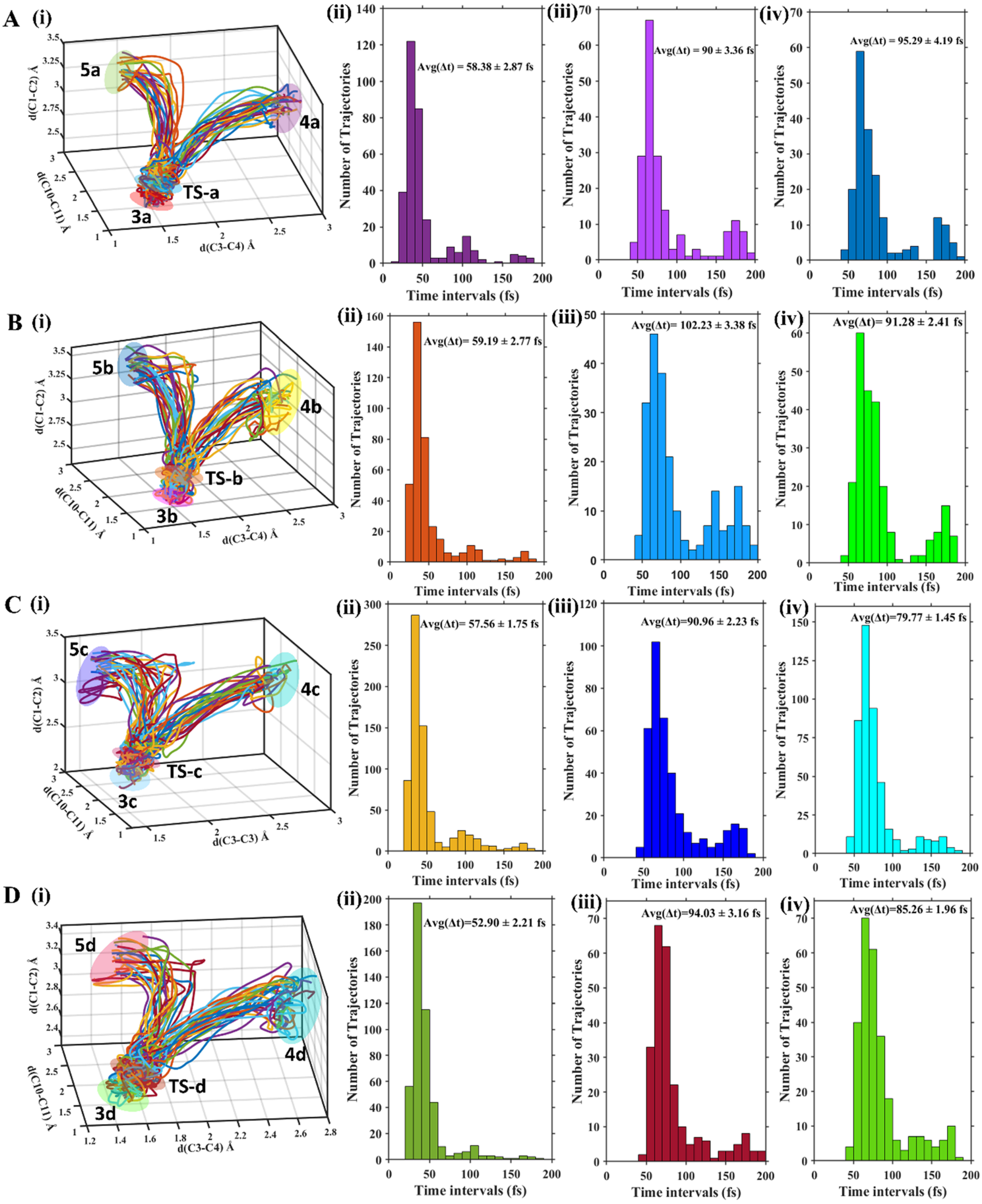

Fig. 3 (i) 50 representative trajectories for the formation of **4** and **5** from **3** and average time required for (ii) **3** → **TS**, (iii) **TS** → **4**, and (iv) **TS** → **5** for **3(a–d)** in (A), (B), (C) and (D), respectively.

more symmetrical. Formally, the monosubstituted **3** has only C_1 symmetry (see Table 2) while the bi-substituted ones preponderantly have a C_s point-group.[47] Comparing the mono and bi-fluorine substituted analogues in **3e** and **3f,** respectively, the percentage of the dynamical product sharply decreases from 47% to 29%. Analogously, for mono and bi-substituted –Cl groups in **3g** and **3h**, the contribution of the bridgehead substituted products are 41% and 25%, respectively. Similarly, one observes a strong correlation with asymmetrical functional group substitutions for $-CH_3$, –CN, $-NO_2$, –Ph and $-NMe_2$. The percentages of dynamical products for the mono substituted analogues are 48%, 37%, 53%, 56% and 53% while the same for bi-substitutions are 36%, 15%, 15%, 12% and 13% only. Fig. 4 shows the sharp reduction in the dynamical product (bridgehead substituted product) formation as the substitution in the rings become more symmetric.

Table 3 Trajectory analyses, product ratio, reaction free energy and free energy of activation at 298.15 K for the monosubstituted and bi-substituted *endo*,*endo*-9,10-diazatetracyclo[3.3.2.0^{2,4}.0^{6,8}]dec-9-ene (**3e–3o**) at the M062X/6-31G(d) level of theory

Entry	Reactant 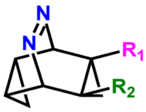	Total trajectories	Productive trajectories	Trajectories reached **4**	Trajectories reached **5**	**4** : **5**	$\Delta G^{\ddagger}_{3\rightarrow4}$ (kcal mol^{-1})	ΔG_4 (kcal mol^{-1})	ΔG_5 (kcal mol^{-1})	$\Delta G^{\ddagger}_{4\rightarrow5}$ (kcal mol^{-1})
3e	R_1 = F, R_2 = H	269	244	129	115	1.12 : 1	7.6	−68.4	−65.2	19.2
3f	R_1 = F, R_2 = F	262	240	171	69	2.48 : 1	6.6	−77.3	67.3	24.3
3g	R_1 = Cl, R_2 = H	392	368	218	150	1.45 : 1	7.7	−66.7	−64.3	18.2
3h	R_1 = Cl, R_2 = Cl	422	389	291	98	2.97 : 1	7.7	−70.5	−62.7	20.1
3i	R_1 = CH_3, R_2 = H	488	446	234	212	1.10 : 1	8.0	−64.4	−63.3	17.2
3j	R_1 = CH_3, R_2 = CH_3	604	554	354	200	1.77 : 1	8.5	−65.2	−60.6	18.7
3k	R_1 = CN, R_2 = H	408	369	231	138	1.67 : 1	7.8	−68.2	−65.0	16.5
3l	R_1 = CN, R_2 = CN	324	298	251	47	5.34 : 1	7.5	−74.1	−64.9	18.5
3m	R_1 = NO_2, R_2 = NO_2	379	351	299	52	5.75 : 1	6.6	−76.8	−65.6	21.9
3n	R_1 = Ph, R_2 = Ph	431	398	341	49	6.96 : 1	10.6	−66.5	−62.2	15.4
3o	R_1 = NMe_2, R_2 = NMe_2	332	313	272	41	6.63 : 1	10.0	−67.4	−54.7	16.5

To understand the preference of the mono-substituted **3** towards the dynamical products we have analysed the minimum energy pathway (MEP) along the intrinsic reaction coordinate (IRC). Comparing the MEP *vs.* IRC for the mono and bi-substituted analogues in Fig. 5, we observe that post the transition-state, the doubly substituted molecules descend steeply towards the product. On the other hand, the mono-substituted compounds exhibit a much flatter and plateaued potential energy surface beyond the TS. The greater slope in the case of the former ensures that from the transition-state the molecules have a greater tendency to fall in the product **4** zone (cyclohexadienyl substituted product) and the possibility for bifurcation post-TS is reduced. This suppresses the bridgehead substituted product, **5**. This can also be understood from the bond-strengths of the C3–C4/C10–C11 bonds (see Fig. 2) in the TSs. For the mono-substituted cases, NBO analyses (see Table S4, ESI†) for the TS-structures show that the % s-character for the C3–C4 bond > C10–C11 bond, which implies that the C3–C4 bond is stronger than the C10–C11 bond. Therefore, cleavage of the C10–C11 bond should be relatively easier compared to C3–C4. As a result, the fraction of dynamical product **5** is relatively higher. But for the doubly substituted cases the situation gets reversed. The % s-character becomes smaller for the C3–C4 bond than the C10–C11 bond. Therefore, the cyclohexadienyl substituted product **4** gets preference. Additionally, comparing the product stability between the cyclohexadienyl substituted and bridgehead substituted products, the free energy difference $\Delta\Delta G$(**4**–**5**) is much higher (5–13 kcal mol^{-1}) for the doubly substituted cases with respect to the mono-substituted ones (1–3 kcal mol^{-1}). This leads to a steeper MEP for the IRC path in the case of the doubly substituted molecules.

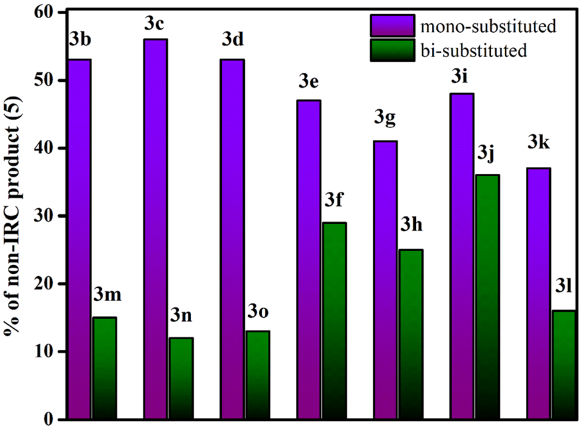

Fig. 4 Comparative profile for the percentage of bridgehead substituted products (**5**) in mono-substituted and bi-substituted *endo*,*endo*-9,10-diazatetracyclo[3.3.2.0^{2,4}.0^{6,8}]dec-9-ene (**3b–3o**).

Experimental detection of post-transition state bifurcation gets facilitated by replacing the lighter isotopes by their heavier isotopologue, like protons by D, carbon by C^{13} and nitrogen by N^{15} *etc.* The product selectivity gets controlled by their differences in masses and this being a purely classical (non-quantum) phenomenon is called the Newtonian kinetic isotope effect (NKIE).[48] The difference in momenta impacts the zero-point energies (ZPE) as well as the vibrational frequencies of the molecules involved in the reaction. QCT trajectory calculations are performed on the H/D, ^{12}C/^{13}C and ^{14}N/^{15}N isotopologues of **3a** (see Fig. 6) and reported in Table 4. In Fig. 6 (**I**), when a single H is substituted by D, the **4** : **5** ∼1 because only one hydrogen is substituted at the distal position by deuterium. However, for bi-substitution in **II**, **4** : **5** = 0.91 : 1 indicating the preference towards the bridgehead substituted product. The higher mass along the C3–C4 bond restricts its bond vibration as a result of which bond opening along C10–C11 gets facile. This favours product **5**. ^{14}N/^{15}N substitution in **III** hardly alters the **4** : **5** ratio from ∼1 as nitrogen is placed remote to

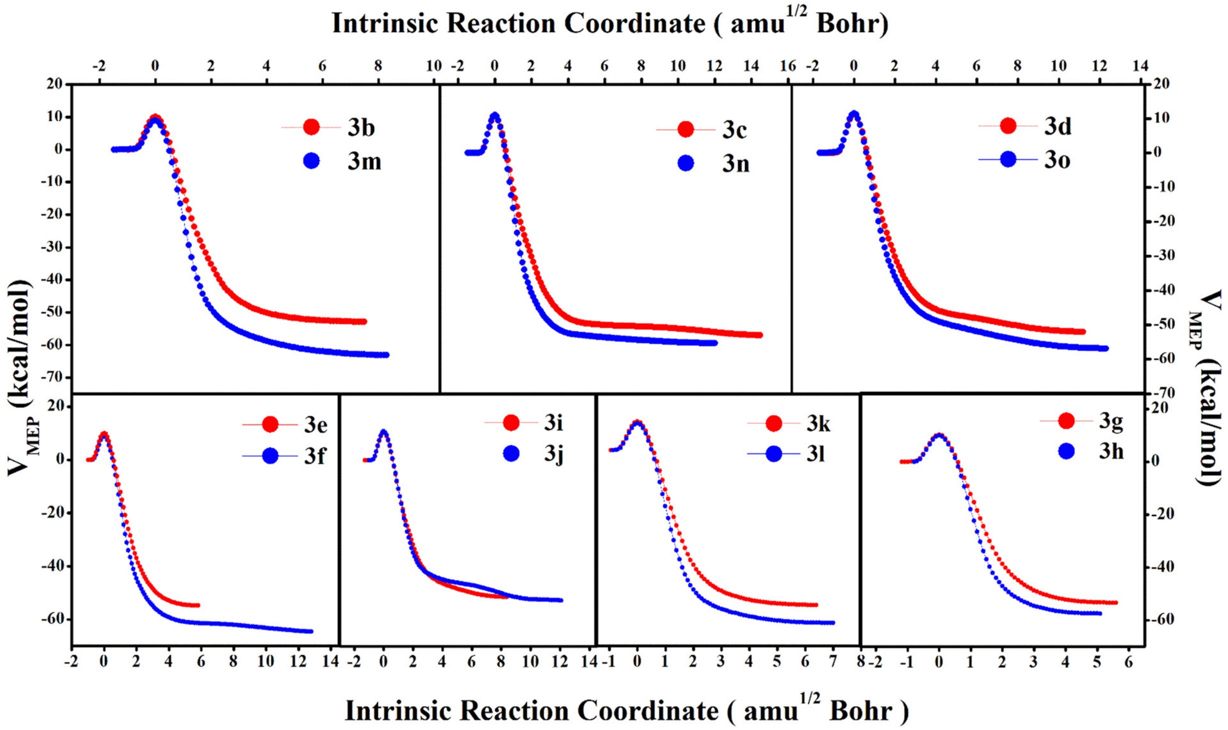

Fig. 5 The minimum energy path along the intrinsic reaction coordinate for **3** → **4** for mono and bi-substituted **3**.

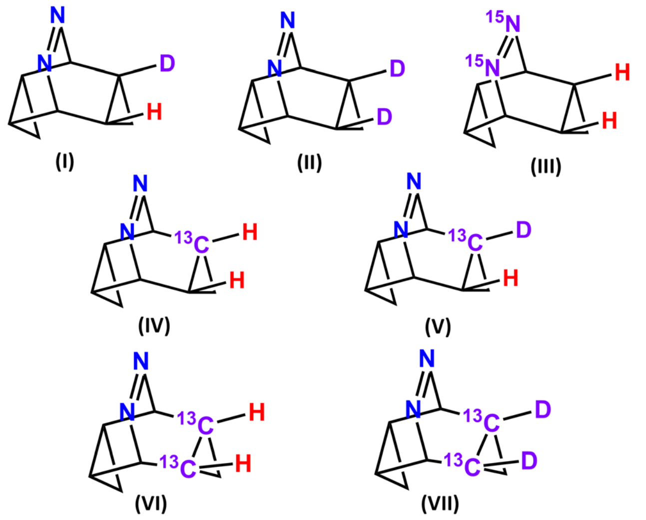

Fig. 6 Seven isotopomers for **3a** on which quasi classical trajectory calculations are performed.

the bond-opening site. A significant effect of isotopic substitution occurs for $^{12}C/^{13}C$ in **IV** as it is the primary bond-cleavage site. Increasing the heaviness of the C3–C4 bond restricts motion along the IRC path and significantly alters the product selectivity towards the dynamical product with **4** : **5** = 0.96 : 1. The effect gets further augmented when D is substituted in the ^{13}C-isotopologue (see **V**) leading to a **4** : **5** = 0.91 : 1. Replacing both the C3 and C4 carbons atoms by ^{13}C augments the KIE to make **4** : **5** as 0.85 in **VI**. The dynamic effects get most pronounced in **VII** where both the carbon and hydrogens are replaced by their heavier isotopes to make **4** : **5** = 0.65.

Dynamic effects get amplified cooperatively as the C3–C4 bond gets substituted by heavier isotopes. For mono-substitution, simultaneous replacement of one C by ^{13}C and the H-atom connected to it in **V** by D, produces **4** : **5** = 0.91 which is lower than the product of the individual **I** and **IV**. Similarly, **4** : **5** for **VII** (= 0.65) < **II** × **VI** (= 0.77).

Conclusions

Post-transition state bifurcation on a potential energy surface produces multiple products. While the product derived from the intrinsic reaction coordinate (IRC) is rather straightforward to envision from the transition-state theory (TST) the same fails to provide a quantitative understanding of the dynamical products. The situation becomes further complicated in molecules with complex topography in the PES. By controlling the slope of the PES beyond the TST, the product selectivity can be dictated. Asymmetry in the functional group substitution makes the surface shallower, thereby increasing the population of the dynamical product. On the other hand, symmetric substitution makes the PES steeper resulting in the expected cyclohexadienyl substituted product. An exalted s-orbital character of the crucial C–C bond can be achieved through asymmetric substitution that favors dynamical products (bridgehead substituted product). Functionalization induced alteration of the PES, therefore, provides an experimentally amenable route

Table 4 Trajectory analyses at 298.15 K for **I–VII** at the M06-2X/6-31G(d) level of theory

Reactant	Total trajectory	Productive trajectory	Trajectory reached **5**	Trajectory reached **6**	**4 : 5**	95% confidence
I	417	382	191	191	1 : 1	1.22–0.81
II	538	511	243	268	0.91 : 1	1.08–0.76
III	1558	1436	727	709	1.02 : 1	1.14–0.92
IV	394	364	178	186	0.96 : 1	1.18–0.78
V	352	327	156	171	0.91 : 1	1.14–0.73
VI	366	331	152	179	0.85 : 1	1.06–0.68
VII	495	461	182	279	0.65 : 1	0.79–0.54

for exact control of the dynamical effects in a reaction. In fact, the product ratio between the cyclohexadienyl substituted and bridgehead substituted products can be tuned either way just by the symmetry of the substitution in **3**. Considering the marked difference between the fate of the reaction, the trade-off between the cyclohexadienyl substituted product and dynamical product bridgehead substituted alternative can be an excellent test to experimentally determine the non-statistical dynamical role of functional-group asymmetry. Additionally, isotopic substitution provides an alternate route towards magnifying the dynamical aspects in the symmetrically substituted reactants. Therefore, the extent to which non-statistical dynamics can affect reactivity, can be explicitly calibrated through both functional group and isotopic substitutions. We expect that at-least one of the two approaches would be experimentally substantiated for the thermal deazetization in **3**.

Data availability

The data supporting this article have been included as part of the ESI.†

Conflicts of interest

The authors declare no competing financial interests.

Acknowledgements

CH thanks CSIR for the senior research fellowship vide 09/0080(18469)/2024-EMR-I. AD thanks TRC-DST for partial funding.

References

1 G. Sudesh Kumar, *Azo Functional Polymers: Functional Group Approach in Macromolec*, CRC Press, 1992.

2 R. S. Aliabadi and N. O. Mahmoodi, Synthesis and Characterization of Polypyrrole, Polyaniline Nanoparticles and Their Nanocomposite for Removal of Azo Dyes; Sunset Yellow and Congo Red, *J. Cleaner Prod.*, 2018, **179**, 235–245.

3 S. Aiken, R. J. L. Edgar, C. D. Gabbutt, B. M. Heron and P. A. Hobson, Negatively Photochromic Organic Compounds: Exploring the Dark Side, *Dyes Pigm.*, 2018, **149**, 92–121.

4 P. S. Engel, Mechanism of the Thermal and Photochemical Decomposition of Azoalkanes, *Chem. Rev.*, 1980, **80**(2), 99–150.

5 R. A. Bartsch, Y. M. Chae, S. Ham and D. M. Birney, Experimental and Theoretical Studies on the Thermal Decomposition of Heterocyclic Nitrosimines1, *J. Am. Chem. Soc.*, 2001, **123**(31), 7479–7486.

6 D. M. Patterson and J. A. Prescher, Orthogonal Bioorthogonal Chemistries, *Curr. Opin. Chem. Biol.*, 2015, **28**, 141–149.

7 K. Lang and J. W. Chin, Bioorthogonal Reactions for Labeling Proteins, *ACS Chem. Biol.*, 2014, **9**(1), 16–20.

8 D. L. Boger, Diels-Alder Reactions of Heterocyclic Aza Dienes. Scope and Applications, *Chem. Rev.*, 1986, **86**(5), 781–793.

9 D. N. Kamber, L. A. Nazarova, Y. Liang, S. A. Lopez, D. M. Patterson, H.-W. Shih, K. N. Houk and J. A. Prescher, Isomeric Cyclopropenes Exhibit Unique Bioorthogonal Reactivities, *J. Am. Chem. Soc.*, 2013, **135**(37), 13680–13683.

10 H. D. Fühlhuber, C. Gousetis, T. Troll and J. Sauer, Photolysen von tetracyclischen azoverbindungen (,-9,10-diazatetracyclo [3.3.2.02,4.06,8]dec-9-ene) ein leichter zugang zu substituierten homotropilidenen, *Tetrahedron Lett.*, 1978, **19**(41), 3903–3906.

11 R. Dyllick-Brenzinger, J. F. M. Oth, H. D. Fühlhuber, C. Gousetis, T. Troll and J. Sauer, Einfluss von Substituenten Auf Die Gleichgewichtslage Unsymmetrisch Substituierter Und Die Geschwindigkeit Der Valenzisomerisierung Symmetrisch Substituierter Homotropilidene, *Tetrahedron Lett.*, 1978, **19**(41), 3907–3910.

12 C. Gousetis and J. Sauer, Ein beitrag zum mechanismus der photolyse tetracyclischer azoverbindungenx) (*exo*,*exo*-9,10-diazatetracyclo[3.3.2.02,4,06,8]dec-9-ene), *Tetrahedron Lett.*, 1979, **20**(15), 1295–1298.

13 J. Sauer, P. Bäuerlein, W. Ebenbeck, R. Dyllick-Brenzinger, C. Gousetis, H. Sichert, T. Troll and U. Wallfahrer, The Cycloaddition-Cycloelimination Pathway to Homotropilidenes – Synthesis and Properties of Homotropilidenes, *Eur. J. Org. Chem.*, 2001, (14), 2639–2657.

14 J. Sauer, P. Bäuerlein, W. Ebenbeck, C. Gousetis, H. Sichert, T. Troll, F. Utz and U. Wallfahrer, [4+2] Cycloadditions of 1,2,4,5-Tetrazines and Cyclopropenes – Synthesis of 3, 4-Diazanorcaradienes and Tetracyclic Aliphatic Azo Compounds, *Eur. J. Org. Chem.*, 2001, (14), 2629–2638.

15 D. Truhlar and B. Garrett, Variational Transition State Theory, *Annu. Rev. Phys. Chem.*, 1980, **35**, 159–189.

16 B. C. Garrett and D. G. Truhlar, Transition state theory, *Encycl. Comput. Chem.*, 1998, **5**, 3094, DOI: 10.1002/0470845015.CTA014.

17 D. H. Ess, S. E. Wheeler, R. G. Iafe, L. Xu, N. Celebi-Olçüm and K. N. Houk, Bifurcations on Potential Energy Surfaces of Organic Reactions, *Angew. Chem., Int. Ed.*, 2008, **47**(40), 7592–7601.

18 P. Collins, B. K. Carpenter, G. S. Ezra and S. Wiggins, Nonstatistical Dynamics on Potentials Exhibiting Reaction Path Bifurcations and Valley-Ridge Inflection Points, *J. Chem. Phys.*, 2013, **139**(15), 154108.

19 H.-H. Chuang, D. J. Tantillo and C.-P. Hsu, Construction of Two-Dimensional Potential Energy Surfaces of Reactions with Post-Transition-State Bifurcations, *J. Chem. Theory Comput.*, 2020, **16**(7), 4050–4060.

20 S. R. Hare and D. J. Tantillo, Post-Transition State Bifurcations Gain Momentum – Current State of the Field, *J. Macromol. Sci., Part A: Pure Appl. Chem.*, 2017, **89**(6), 679–698.

21 D. J. Tantillo, Beyond Transition State theory—Non-Statistical Dynamic Effects for Organic Reactions, in *Advances in Physical Organic Chemistry*, ed. I. H. Williams and N. H. Williams, Academic Press, 2021, ch. 1, vol. 55, pp. 1–16.

22 Y. J. Hong and D. J. Tantillo, A Potential Energy Surface Bifurcation in Terpene Biosynthesis, *Nat. Chem.*, 2009, **1**(5), 384–389.

23 S. R. Hare, A. Li and D. J. Tantillo, Post-Transition State Bifurcations Induce Dynamical Detours in Pummerer-like Reactions, *Chem. Sci.*, 2018, **9**(48), 8937–8945.

24 K. S. Khuong and K. N. Houk, One-Bond, Two-Bond, and Three-Bond Mechanisms in Thermal Deazetizations of 2, 3-diazabicyclo[2.2.2]oct-2-Enes, Trans-Azomethane, and 2, 3-diazabicyclo[2.2.1]hept-2-Ene, *J. Am. Chem. Soc.*, 2003, **125**(48), 14867–14883.

25 L. Törk, G. Jiménez-Osés, C. Doubleday, F. Liu and K. N. Houk, Molecular Dynamics of the Diels–Alder Reactions of Tetrazines with Alkenes and N2 Extrusions from Adducts, *J. Am. Chem. Soc.*, 2015, **137**(14), 4749–4758.

26 R. Villar López, O. N. Faza and C. Silva López, Dynamic Effects Responsible for High Selectivity in a [3,3] Sigmatropic Rearrangement Featuring a Bispericyclic Transition State, *J. Org. Chem.*, 2017, **82**(9), 4758–4765.

27 M. Castiñeira Reis, C. S. López, O. Nieto Faza and D. J. Tantillo, Pushing the Limits of Concertedness. A Waltz of Wandering Carbocations, *Chem. Sci.*, 2019, **10**(7), 2159–2170.

28 J. I. Wheeler, A. J. Schaefer and D. H. Ess, Trajectory-Based Time-Resolved Mechanism for Benzene Reductive Elimination from Cyclopentadienyl Mo/W Phenyl Hydride Complexes, *J. Phys. Chem. A*, 2024, **128**(24), 4775–4786.

29 N. Mandal and A. Datta, Dynamical Effects along the Bifurcation Pathway Control Semibullvalene Formation in Deazetization Reactions, *J. Phys. Chem. B*, 2018, **122**(3), 1239–1244.

30 N. Mandal, A. Das, C. Hajra and A. Datta, Stereoelectronic and Dynamical Effects Dictate Nitrogen Inversion during Valence Isomerism in Benzene Imine, *Chem. Sci.*, 2022, **13**(3), 704–712.

31 N. Mandal and A. Datta, Gold(I)-Catalyzed Intramolecular Diels–Alder Reaction: Evolution of Trappable Intermediates *via* Asynchronous Transition States, *J. Org. Chem.*, 2018, **83**(18), 11167–11177.

32 E. L. Allred and J. C. Hinshaw, Thermolysis of Azo-Compounds: A Reactivity Factor of 10 17, *J. Chem. Soc. D*, 1969, (18), 1021–1022.

33 M. B. Reyes and B. K. Carpenter, Mechanism of Thermal Deazetization of 2,3-Diazabicyclo[2.2.1]hept-2-Ene and Its Reaction Dynamics in Supercritical Fluids, *J. Am. Chem. Soc.*, 2000, **122**(41), 10163–10176.

34 K. K. Kelly, J. S. Hirschi and D. A. Singleton, Newtonian Kinetic Isotope Effects. Observation, Prediction, and Origin of Heavy-Atom Dynamic Isotope Effects, *J. Am. Chem. Soc.*, 2009, **131**(24), 8382–8383.

35 M. J. Frisch, G. W. Trucks, H. B. Schlegel, G. E. Scuseria, M. A. Robb, J. R. Cheeseman, G. Scalmani, V. Barone, G. A. Petersson, H. Nakatsuji, X. Li, M. Caricato, A. V. Marenich, J. Bloino, B. G. Janesko, R. Gomperts, B. Mennucci, H. P. Hratchian, J. V. Ortiz, A. F. Izmaylov, J. L. Sonnenberg, D. Williams-Young, F. Ding, F. Lipparini, F. Egidi, J. Goings, B. Peng, A. Petrone, T. Henderson, D. Ranasinghe, V. G. Zakrzewski, J. Gao, N. Rega, G. Zheng, W. Liang, M. Hada, M. Ehara, K. Toyota, R. Fukuda, J. Hasegawa, M. Ishida, T. Nakajima, Y. Honda, O. Kitao, H. Nakai, T. Vreven, K. Throssell, J. A. Montgomery, Jr., J. E. Peralta, F. Ogliaro, M. J. Bearpark, J. J. Heyd, E. N. Brothers, K. N. Kudin, V. N. Staroverov, T. A. Keith, R. Kobayashi, J. Normand, K. Raghavachari, A. P. Rendell, J. C. Burant, S. S. Iyengar, J. Tomasi, M. Cossi, J. M. Millam, M. Klene, C. Adamo, R. Cammi, J. W. Ochterski, R. L. Martin, K. Morokuma, O. Farkas, J. B. Foresman and D. J. Fox, *Gaussian 16, Revision C.01*, Gaussian, Inc., Wallingford CT, 2016.

36 Y. Zhao and D. G. Truhlar, The M06 Suite of Density Functionals for Main Group Thermochemistry, Thermochemical Kinetics, Noncovalent Interactions, Excited States, and Transition Elements: Two New Functionals and Systematic Testing of Four M06-Class Functionals and 12 Other Functionals, *Theor. Chem. Acc.*, 2008, **120**(1), 215–241.

37 P. C. Hariharan and J. A. Pople, The Influence of Polarization Functions on Molecular Orbital Hydrogenation Energies, *Theor. Chim. Acta*, 1973, **28**(3), 213–222.

38 K. Fukui, The Path of Chemical Reactions – the IRC Approach, *Acc. Chem. Res.*, 1981, **14**(12), 363–368.

39 A. Becke, A New Mixing of Hartree-Fock and Local Density-Functional Theories, *J. Chem. Phys.*, 1993, **98**, 1372–1377.

40 V. A. Rassolov, M. A. Ratner and J. A. Pople, 6-31G* Basis Set for Third-row Atoms, *J. Comput. Chem.*, 2001, **22**(9), 976–984.

41 S. Grimme, J. Antony, S. Ehrlich and H. Krieg, A Consistent and Accurate Ab Initio Parametrization of Density Functional Dispersion Correction (DFT-D) for the 94 Elements H-Pu, *J. Chem. Phys.*, 2010, **132**(15), 154104.

42 C. Riplinger, B. Sandhoefer, A. Hansen and F. Neese, Natural Triple Excitations in Local Coupled Cluster Calculations with Pair Natural Orbitals, *J. Chem. Phys.*, 2013, **139**(13), 134101.

43 C. Riplinger, B. Sandhoefer, A. Hansen and F. Neese, Natural Triple Excitations in Local Coupled Cluster Calculations with Pair Natural Orbitals, *J. Chem. Phys.*, 2013, **139**(13), 134101.

44 E. Schiavo, K. Bhattacharyya, M. Mehring and A. A. Auer, Are Heavy Pnictogen-π Interactions Really "π Interactions"?, *Chemistry*, 2021, **27**(58), 14520–14526.

45 F. Neese, Software Update: The ORCA Program System—Version 5.0, *Wiley Interdiscip. Rev.: Comput. Mol. Sci.*, 2022, **12**(5), e1606.

46 D. A. Singleton, C. Hang, M. J. Szymanski and E. E. Greenwald, A New Form of Kinetic Isotope Effect. Dynamic Effects on Isotopic Selectivity and Regioselectivity, *J. Am. Chem. Soc.*, 2003, **125**(5), 1176–1177.

47 For **3m**, the flexibility of rotations along the $-NO_2$ groups causes symmetry-breaking from C_s to C_1 point-group.

48 Note that the Newtonian kinetic isotope effect is a purely classical momentum driven process and differs from kinetic isotope effects (both primary and secondary) where quantum mechanical tunnelling also plays a significant role. See, S. Karmakar and A. Datta, Heavy-atom Tunneling in Organic Transformations, *J. Chem. Sci.*, 2020, **132**, 127, DOI: 10.1007/s12039-020-01809-x.